Preliminary study of the $\gamma\gamma \to \tau^+\tau^-$ process for the measurement of the tau anomalous magnetic moment in a hadron collider

CERN Summer School

Juan Pablo Garcés

Supervisors:

Dr. Chiara Roda

Dr. Monica Verducci

August 2021

Contents

1. Abstract

The recent measurement of the muon's anomalous magnetic moment by the Fermilab experiment "Muon g-2" shows a 4.2σ discrepancy with the theoretical prediction based on the Standard Model, serving as huge motivation for the study of new physics. An example of the later consists in using ATLAS to perform the measurement of the anomalous magnetic moment of the tau lepton (a_τ), using tau lepton pairs produced in photon-photon collisions generated from lead ions interactions (PbPb$\rightarrow$ PbPb$\gamma\gamma \rightarrow \tau^+\tau^-$). In this work we analyze the distributions of different observables from simulated tau leptons produced via this process and their most frequent charged decay products. This is done using MadGraph and Pythia8 generators, while the detector effects are introduced with Delphes. We compare the results obtained for a sample including only Standard Model (SM) physics and another one with additional Beyond the Standard Model (BSM) effects due to a non-zero a_τ. Finally, the most abundant leptonic backgrounds processes $\gamma\gamma \rightarrow e^+e^-/\mu^+\mu^-$ are also generated and compared to the signal-only samples with the aim of shedding some light toward possible cuts for the reconstruction of tau decays.

2. Introduction

Until now, the Standard Model (SM) has been incredibly successful in predicting physical quantities that agree extremely well with experiments. However, as satisfying as that has been, it is of common knowledge among the scientific community that the SM is not the final answer to the quest of the underlying framework of nature.

As a consequence of the above, lots of efforts have been invested in looking for quantities for which SM predictions and experimental measurements disagree enough as to indicate the existence of physics beyond the standard model (BSM). A promising example of this is the anomalous magnetic dipole moment of the muon (a_μ), which is already known to disagree with measurement in 4.2σ (Ref. [9]).

Along the same lines is the study of a_τ, with the difference that the τ is about 17 times heavier and its lifetime is about 10^7 times shorter, making it impossible to detect by means of the spin precession method used in the "Muon g-2" experiment for muons. However, its bigger mass makes it much more sensitive to BSM physics than the μ, giving enough motivation to indirect studies of its anomalous magnetic dipole moment: $a_\tau = \frac{1}{2}(g_\tau - 2)$.

The major aim of this work is to contribute to the indirect study of a_τ by looking into the effects that it has on distributions for different observables obtained from simulated $\gamma\gamma \rightarrow \tau^+\tau^-$ events. The samples we study are based on MadGraph for the event generation and Pythia8 for tau decay, particle shower and hadronisation (Ref. [5] and [10]).

A second aim of this work is to quantify how efficient we are in reconstructing tracks of final state particles (f.s.p) coming from tau decays, by simulating the detector effects with Delphes (Ref. [3]). We also simulate background events $\gamma\gamma \rightarrow e^+e^-/\mu^+\mu^-$ to compare with the signal-only sample, so that when we encounter real data we can have informed kinematical constraints that can help subtracting those background processes.

3. Previous remarks

In this section we give brief descriptions of the most important physical concepts and software tools that are fundamental for this analysis.

3.1. Magnetic dipole moment

Elementary particles carry an intrinsic angular momentum called "spin" ($\vec{S}$) and it is related to the magnetic dipole moment ($\vec{\mu}$) of that particle according to:

$$\vec{\mu} = g\frac{e}{2m_e}\vec{S}$$

where g is the Landé factor, which takes the value of 2 in Dirac theory and describes the lowest order interaction of the particle's magnetic moment with the photon.

The *anomalous magnetic dipole moment* (a_l) quantifies the deviation from $g = 2$ according to

$$a_l = \frac{g_l - 2}{2}$$

where l stands for lepton (e, μ or τ). These deviations are due to diagrams of orders higher than α^2 (Dirac theory), where virtual electromagnetic, weak and hadronic processes contribute with corrections calculable within the Standard Model (SM) with very high precision. However, when these calculations deviate enough from measurement (e.g. a_μ) they motivate the study of BSM models including, for example, the existence of new particles that would explain such discrepancy (see Figure 1).

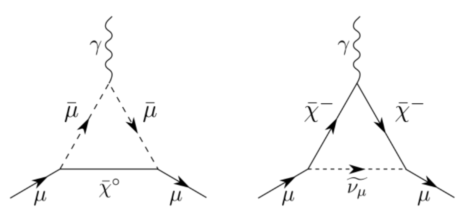

Figure 1: Example of SUSY particles contributing to correction of muon-photon interaction.

In the particular case of the τ, adding higher order corrections within the SM gives:

$$a_\tau^{SM} = a_\tau^{QED} + a_\tau^{EW} + a_\tau^{HAD} = 117721(5) \times 10^{-8}$$

While the experimental limits from DELPHI at the Large Electron Positron Collider based on the process $e^-e^+ \rightarrow e^-e^+\tau^-\tau^+$ are (Ref. [8]):

$$-0.052 < a_\tau^{exp} < 0.013 \quad (95\%CL)$$

which clearly shows the poor level of constraint we currently have on a_τ compared to the SM predicted value. More detailed information on a_τ limits can be found in Ref. [1] and are summarized in Figure 2.

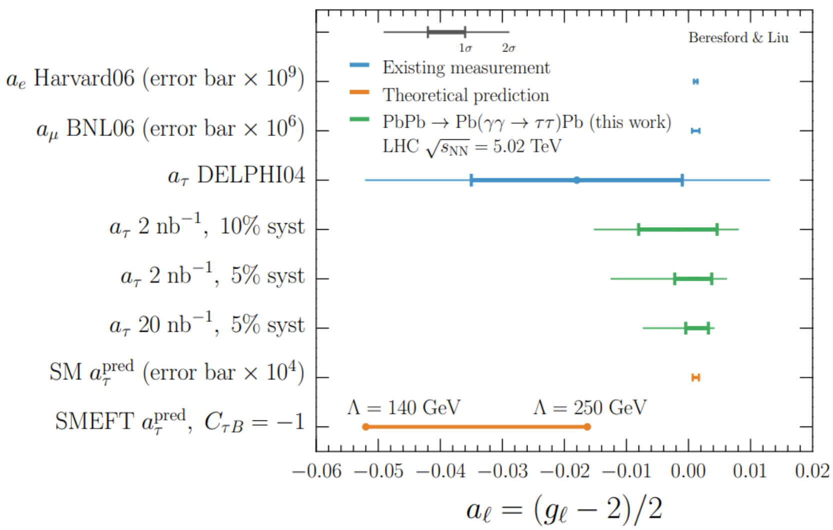

Figure 2: Summary on a_{tau} ranges from previous work (Ref. [1]).

3.2. SM+BSM Lagrangian

In the SM the interaction of the tau's spin angular momentum with the photon field strength ($F_{\mu\nu}$) involves a lagrangian $\mathcal{L}$ including the spinor tensor structure $\sigma^{\mu\nu} = i[\gamma^\mu, \gamma^\nu]/2$, the tau spinors $\tau_{L,R}$ and the tau anomalous magnetic (a_τ) and electric (d_τ) dipole moments:

$$\mathcal{L} = \frac{1}{2}\bar{\tau}_L \sigma^{\mu\nu}(a_\tau \frac{e}{2m_\tau} - id_\tau\gamma_5)\tau_R F_{\mu\nu}$$

BSM modifications affecting a_τ and d_τ are introduced using SM effective field theory (see Ref. [8]). The corrections to a_τ and d_τ are parametrized as function of two real parameters $|C_{\tau B}|$ and φ according to:

$$\delta a_\tau = \frac{2m_\tau}{e}\frac{|C_{\tau B}|}{M}cos\varphi, \qquad \delta d_\tau = \frac{|C_{\tau B}|}{M}sin\varphi$$

3.3. Photon flux

A very important step of the process under analysis is the emission of photons from the lead ions which then fuse to produce the tau pairs. The cross section for the consecutive processes of photon emission from lead (PbPb→ PbPb$\gamma\gamma$) followed by photon fusion into products ($\gamma\gamma \to XX$) is modeled in a way that is analogous to the description of partons in terms of the PDFs. In short, the cross section $\sigma^{PbPb}_{\gamma\gamma\to XX}$ is obtained as the convolution of the cross section for the single $\gamma\gamma \to XX$ process ($\sigma_{\gamma\gamma\to XX}$) with the photon flux ($n(x)$) generated from the lead ions:

$$\sigma^{PbPb}_{\gamma\gamma\to XX} = \int dx_1 dx_2 n(x_1) n(x_2) \sigma_{\gamma\gamma\to XX}$$

where $x_i = E_i/E_{beam}$ and E_i is the energy of the photon emitted from ion i.

In this work the photon fluxes are implemented through MadGraph, and more specific information on $n(x)$ can be found in Ref. [1].

3.4. τ branching ratios

The process of interest in this study is well exemplified by the Feynman diagram shown in Figure 3.

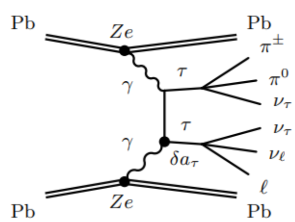

Figure 3: Diagram of tau lepton pair production in ultraperipheral lead ion collsions. Lead ions emit photons which fuse to produce a tau pair. Each tau can then decay hadronically or leptonically.

The most important τ branching fractions according to the PDG (Ref. [7]) are summarized in Table 1.

Process	Branching fraction
$\tau^- \to e^- \bar{\nu}_e \nu_\tau$	17.85%
$\tau^- \to \mu^- \bar{\nu}_\mu \nu_\tau$	17.36%
$\tau^- \to \pi^- \nu_\tau n\pi^0$ (n=0,1,2,3)	46.75%
$\tau^- \to 2\pi^- \pi^+ \nu_\tau n\pi^0$ (n=0,1)	13.91%
$\tau^- \to K^- \nu_\tau n\pi^0$ (n=0,1,2,3)	1.24%

Table 1: Most probable tau decays.

These processes account for 97% of the decay probabilities for τ.

3.5. Simulation steps and software tools

In order to study the characteristics of the PbPb$\rightarrow$ PbPb$\gamma\gamma$ $\rightarrow$ $\tau^+\tau^-$ $\rightarrow$ $f.s.p$ events different simulation softwares are used. A brief description of each of them is given below:

- **MadGraph**: performs simulation of high-energy particle collisions up to next-to-next to leading order. It receives as an input a set of parameters that allow the user to define the initial particles and the type of elementary process to simulate. Most of the parameters of the underlying theory (e.g. masses and couplings) may also be adjusted from the user. This flexibility enables a vast number of phenomenological studies and serves as a guide for analysis of real data. The program outputs the data (e.g. energy, position, momentum and particle type) of all products of the collision, and is formatted (LHE file) in such a way that further processes like particle decays, parton showering and hadronisation can be performed using another software such as Pythia8.
- **Pythia8**: is a general purpose Monte-Carlo generator that can be used to simulate collision events and related processes such as parton showering, hadronisation, multiparton interactions, initial and final state radiation and decays, among others. It uses pQCD and models to transform quarks and gluons to the mesons and baryons that we detect in experiments.
- **Delphes**: takes as input the output files (e.g. HepMC and LHEF) from an event generator and simulates the effect and response of a general purpose collider detector, including a tracking system with a magnetic field, electromagnetic and hadronic calorimeters and a muon identification system. The simulation accounts for the fact that the detector's resolution is subjected to particles interacting with the matter from which the detector is made of, which results in a smearing of the energy and momentum of the particle. The output allows access to reconstructed objects such as tracks, jets, missing energy, reconstructed muons, photons and isolated electrons.
- **Root**: object-oriented program mostly written in C++ and developed by CERN as a tool for particle physics data analysis. It contains several libraries for data visualization and data formatting.

3.6. Simulated data samples

For the present study, MadGraph and DelphesPythia8 were used to simulate 3 samples with 200k $\gamma\gamma \rightarrow \tau^+\tau^- \rightarrow f.s.p$ events each. The first two samples are both based on SM physics while the third includes SM, BSM ($a_\tau = 0.2$) and their interference. One of the SM samples has initial state radiation (ISR) and multiparton interactions (MPI) turned on, while the other one has these processes turned off. ISR is the process by which pre-colliding particles emit radiation in the form of gluons or photons. These gluons then shower, acting as an independent source of f.s.p. On the other hand, MPI accounts for the fact that the colliding protons in LHC contain several partons, and more than one pair can be brought into collision in the same p-p collision. If we want to analyze $\gamma\gamma \rightarrow \tau^+\tau^- \rightarrow f.s.p$ as cleanly as possible we may turn ISR and MPI off. In order to investigate the properties of the leptonic background processes, a sample with 200k $\gamma\gamma \to e^+e^-/\mu^+\mu^-$ events was also simulated.

3.7. Detector setup

Table 2 lists lifetimes and decay lengths for the most abundant particles generated in the process under study. The last column in Table 2 indicates which particles have a long enough lifetime to reach the detector before decaying. For example, the tau leptons decay before reaching the detector and therefore can only be observed by detecting its decay products.

Particle	$\sim$ Lifetime (τ [s])	$\sim$ Decay length (L_{decay} [m])	Status = 1
μ	10^{-6}	10^3	yes
$\pi^\pm$	10^{-8}	10	yes
$K^\pm$	5×10^{-9}	5	yes
K_L^0	10^{-8}	15	yes
π^0	10^{-16}	10^{-4}	no
$\tau^\pm$	10^{-13}	10^{-6}	no

Table 2: Final state partciles' lifetimes and decay lengths and whether they make it to the detector (Status==1) or not.

DelphesPythia8 will assign "Status=1" to final state particles, i.e. to those particles that are stable enough to get to the detector. We have omitted stable particles that don't decay, such as e and γ and unstable particles that we don't analyze below.

The detector effects on what is measured is frequently characterized by its *acceptance* and its *efficiency*. The acceptance considers, the fact that detectors can't cover all accessible space, and therefore some f.s.p can't be measured by it. This highly depends on the geometry of the detector. On the other hand, the efficiency quantifies the probability that a particle that arrives at the detector gets reconstructed correctly. In short, both measurables are calculated by taking the ratio between reconstructed and generated particles, but the efficiency applies the required cuts to the number of generated particles, so it includes only those within the geometrical acceptance of the detector.

Since DELPHES is a fast detector simulation the reconstruction efficiency is simulated through a table that considers the detector geometry and particle type. Table 3 lists the ATLAS tracking efficiencies for the particles we are interested in as described in DELPHES.

Cuts/Particle	Charged hadron	Electron	Muon
$p_T <= 0.1$	0.00	0.00	0.00
$\|\eta\| <= 1.5 \wedge 0.1 < p_T <= 1.0$	0.70	0.73	0.75
$\|\eta\| <= 1.5 \wedge 1.0 < p_T <= 100.0$	0.95	0.95	0.99
$\|\eta\| <= 1.5 \wedge 100.0 < p_T$	0.95	0.99	0.99
$\|\eta\| > 1.5 \wedge \|\eta\| <= 2.5 \wedge 0.1 < p_T <= 1.0$	0.60	0.50	0.70
$\|\eta\| > 1.5 \wedge \|\eta\| <= 2.5 \wedge 1.0 < p_T <= 100.0$	0.85	0.83	0.98
$\|\eta\| > 1.5 \wedge \|\eta\| <= 2.5 \wedge 100.0 < p_T$	0.85	0.90	0.98
$\|\eta\| > 2.5$	0.00	0.00	0.00

Table 3: Tracking detector efficiencies defined in the Delphes run card used to simulate the ATLAS detector.

4. Results and discussion

In subsection 4.1. we evaluate the consistency of our simulation and analysis. Then, in 4.2. we make a comparison between the different simulated data sets based on their distributions for different observables such as transverse momentum, rapidity and di-tau system properties. Finally, in 4.2. we study the tau decays subject to fiducial constraints of the ATLAS detector.

4.1. Simulation and analysis consistency validation

4.1.1. Branching fractions (SM vs SM+BSM)

The branching fractions obtained from the simulated samples are shown in Table 6 and are in good agreement to what was expected from the PDG values (Table 1).

Process	SM (%)	SM+BSM (%)
$\tau^- \to e^- \bar{\nu}_e \nu_\tau$	17.78	17.73
$\tau^- \to \mu^- \bar{\nu}_\mu \nu_\tau$	17.33	17.35
$\tau^- \to \pi^- \nu_\tau n\pi^0$ (n=0,1,2,3)	46.47	46.30
$\tau^- \to 2\pi^- \pi^+ \nu_\tau n\pi^0$ (n=0,1)	14.30	14.44
$\tau^- \to K^- \nu_\tau n\pi^0$ (n=0,1,2,3)	1.20	1.24

Table 4: Branching fractions calculated from SM and SM+BSM samples.

4.1.2. Detector tracking efficiency

As a first step to quantify how efficient we are in reconstructing the f.s.p of our interest (electrons, muons and charged pions) we calculate the ratios between the number of generated particles (Gen) and reconstructed tracks (Rec). Now, before taking the ratio we select only those generated particles that make it to the detector, i.e. we get rid of the geometrical limitations of our detector and focus only on how likely our detector is in reconstructing correctly a certain track given that the generated particle producing the track actually made it to the detector. To be specific, the efficiency ϵ is given by the ratio between the number of reconstructed tracks N_{rec} to the number of generated particles satisfying the condition $|\eta| < 2.5$ ($N_{gen}^{|\eta|<2.5}$): $\epsilon = \frac{N_{rec}}{N_{gen}^{|\eta|<2.5}}$.

The calculated efficiency values as function of the transverse momentum together with the histograms involved in the calculation can be visualized in the plots shown in Figure 4.

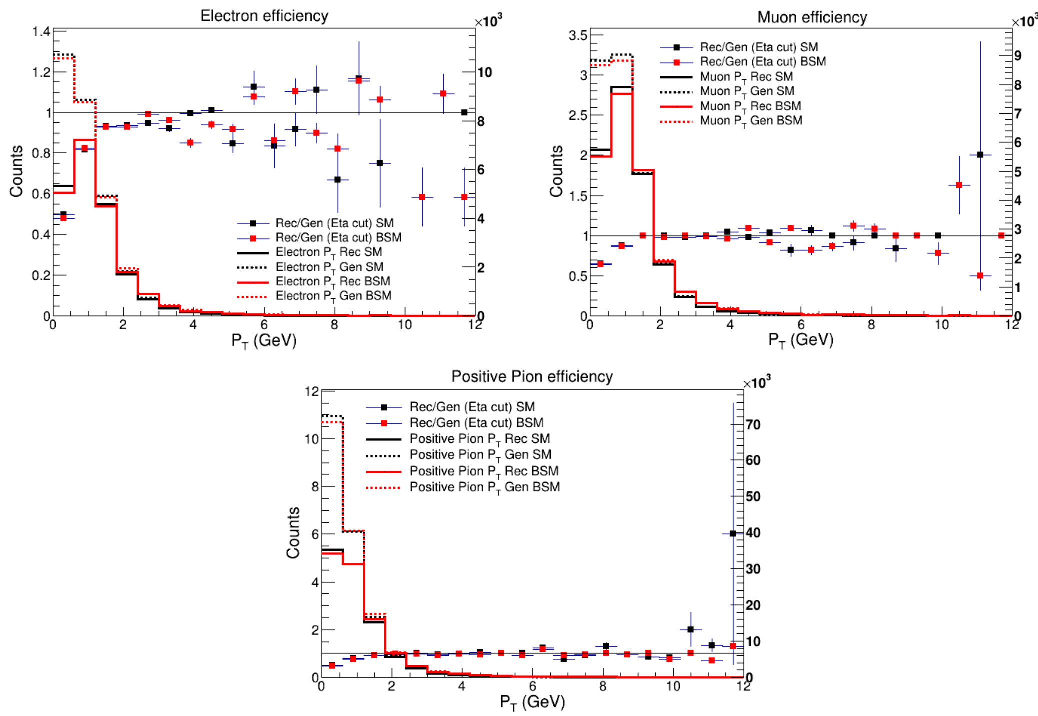

Figure 4: Tracking efficiencies for e^-, μ^- and π^+ (scatter plot and left vertical axis) and the p_T distributions used to get those efficiencies (histograms and right axis).

Having efficiencies greater than one would mean that we have more observed tracks than generated charged particles. One possibility could be that the simulation includes track fragmentation, and in order to investigate whether this is the case we count the number generated charged particles satisfying $|\eta| < 2.5$ and the number of reconstructed tracks among the SM sample and summarize the results in Table 7 for e^-, μ^- and π^+.

Particle	$n_{trk} < n_{gen}$	$n_{trk} = n_{gen}$	$n_{trk} > n_{gen}$
e^-	10,003	189,997	0
μ^-	6,672	193,328	0
π^+	50,191	149,808	1

Table 5: Number of events among the SM sample for which there was a lower, equal or greater number of generated particles with $|\eta| < 2.5$ than reconstructed tracks.

Table 7 is clear proof that we can rule out the possibility of attributing the fact of having efficiencies greater than one due to a higher number of reconstructed tracks than generated particles. Another possibility is that these nonphysical values of efficiencies are product of low statistics and bin migration due to p_T smearing from the track measurements. Purity tests could be performed to check this hypothesis. For those regions where the statistics are high enough, i.e. for p_T lower than 3-4 GeV, no efficiencies greater than one are obtained. Among these p_T regions the efficiencies start at approximately 0.5 GeV and approach unity monotonically as p_T increases.

Finally, Table 8 shows the calculated tracking efficiencies among the SM sample for different η and p_T bins and their relative deviation to the Delphes run card values (Table 3).

Cuts/Particle	$\epsilon(\pi^+)$	$\epsilon(e^-)$	$\epsilon(\mu^-)$
$p_T <= 0.1$	0.00	0.00	0.00
$\lvert\eta\rvert <= 1.5 \wedge 0.1 < p_T <= 1.0$	0.59	0.67	0.73
$\lvert\eta\rvert <= 1.5 \wedge 1.0 < p_T <= 100.0$	0.95	0.96	0.99
$\lvert\eta\rvert <= 1.5 \wedge 100.0 < p_T$	0.95	-	0.99
$\lvert\eta\rvert > 1.5 \wedge \lvert\eta\rvert <= 2.5 \wedge 0.1 < p_T <= 1.0$	0.60	0.61	0.75
$\lvert\eta\rvert > 1.5 \wedge \lvert\eta\rvert <= 2.5 \wedge 1.0 < p_T <= 100.0$	0.84	0.84	0.99
$\lvert\eta\rvert > 1.5 \wedge \lvert\eta\rvert <= 2.5 \wedge 100.0 < p_T$	0.84	-	0.99
$\lvert\eta\rvert > 2.5$	0.00	0.00	0.00
Avg. rel. deviation	2.3%	5.4%	1.5%

Table 6: Tracking efficiencies calculated using the SM sample for different $\eta \times p_T$ bins and their average relative deviation with respect to the Delphes run card values.

4.2. Kinematical comparison of SM, SM+BSM and Bkg

4.2.1. SM vs. SM+BSM vs. Bkg (f.s.p)

As discussed in the section A.1. of the appendix, MPI and ISR effects are not appropriate in the case of ultraperipheral Pb-Pb collisions, and therefore we base our analysis on samples with these processes turned off. In this case all the f.s.p are generated from tau decays either directly or through intermediate decays. The Pythia8 run card specifying the configuration used to simulate the decays, radiation and showering processes (among other things) for all these samples is included in the section A.2. of the appendix. Also, the total cross sections obtained for each sample is specified in Table 5.

Sample	Cross Section (pb)
SM ($a_\tau = 0$)	$6.4836 \times 10^8 \pm 5.0 \times 10^5$
SM+BSM ($a_\tau = 0.2$)	$1.2617 \times 10^9 \pm 9.6 \times 10^6$
Bkg	$8.5161 \times 10^9 \pm 5.3 \times 10^6$

Table 7: Total cross sections for the different simulated samples.

For simplicity we call the Standard Model sample MPI=ISR=off "SM", the sample including BSM effects with $a_\tau = 0.2$ "SM+BSM" and the background-only sample "Bkg". Figure

5 shows plots of p_T for e^-, μ^- and π^+ among these three samples. The y distirbution is only shown for e^- due to its similarity to the same distribution for the other particles. In all plots the bottom panels show the ratio between the SM+BSM and SM distributions.

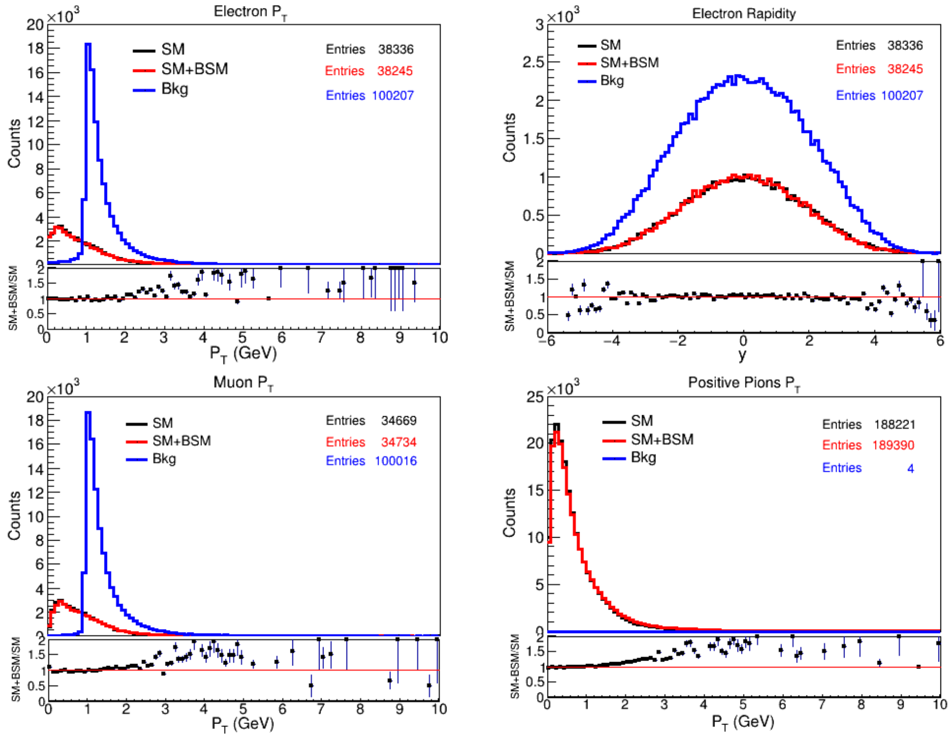

Figure 5: e^-, μ^- and π^+ transverse momentum and rapidity for the SM, SM+BSM and Bkg samples (top pad). Ratio between SM+BSM over SM distributions (bottom pad)

The bottom panels in the p_T plots show that the SM+BSM sample has systematically more f.s.p at high transverse momenta than the SM sample, while the ratio in rapidity remains flat along the high-statistics ($|y| < 2.5$) region. Also, for the p_T distributions, there is a clear difference in the shape and peak location between the signal (SM and SM+BSM) and background (Bkg) samples. The background distribution peaks close to 1.1 GeV and has a mean of 1.45 GeV while the signal distributions peak around 0.3 GeV and have a mean of 0.93 GeV. Therefore, the signal f.s.p are expected to be predominantly softer in p_T that the f.s.p coming from the background processes $\gamma\gamma \to e^+e^-/\mu^+\mu^-$.

4.2.2. SM vs. SM+BSM (τ)

We now focus on the observable distributions of the tau leptons instead of the f.s.p they produce. Even-though we measure the tau products instead of the taus themselves, looking at these distributions can still give us some insights regarding the effects of $a_\tau \neq 0$.

In Figure 6 we show different distributions for the two-tau system and the taus themselves together with the ratios between the SM+BSM and SM samples. The SM+BSM sample has substantially more tau pairs at higher masses and at higher transverse momenta. For example, in the range of the Higgs mass between 120-130 Gev we have one entry for the

SM sample and 5 for the SM+BSM sample. Also, while the tau leptons in the SM sample have a cut-off in p_T a little before 30 GeV, the SM+BSM sample has taus with p_T higher than 50 GeV and it already has four times the differential cross section of SM at 10 GeV from where the ratio keeps increasing for higher p_T. On the other hand, the p_T and y distributions of the tau pairs are fairly similar in shape for both samples, and so are the single-tau y and ϕ distributions.

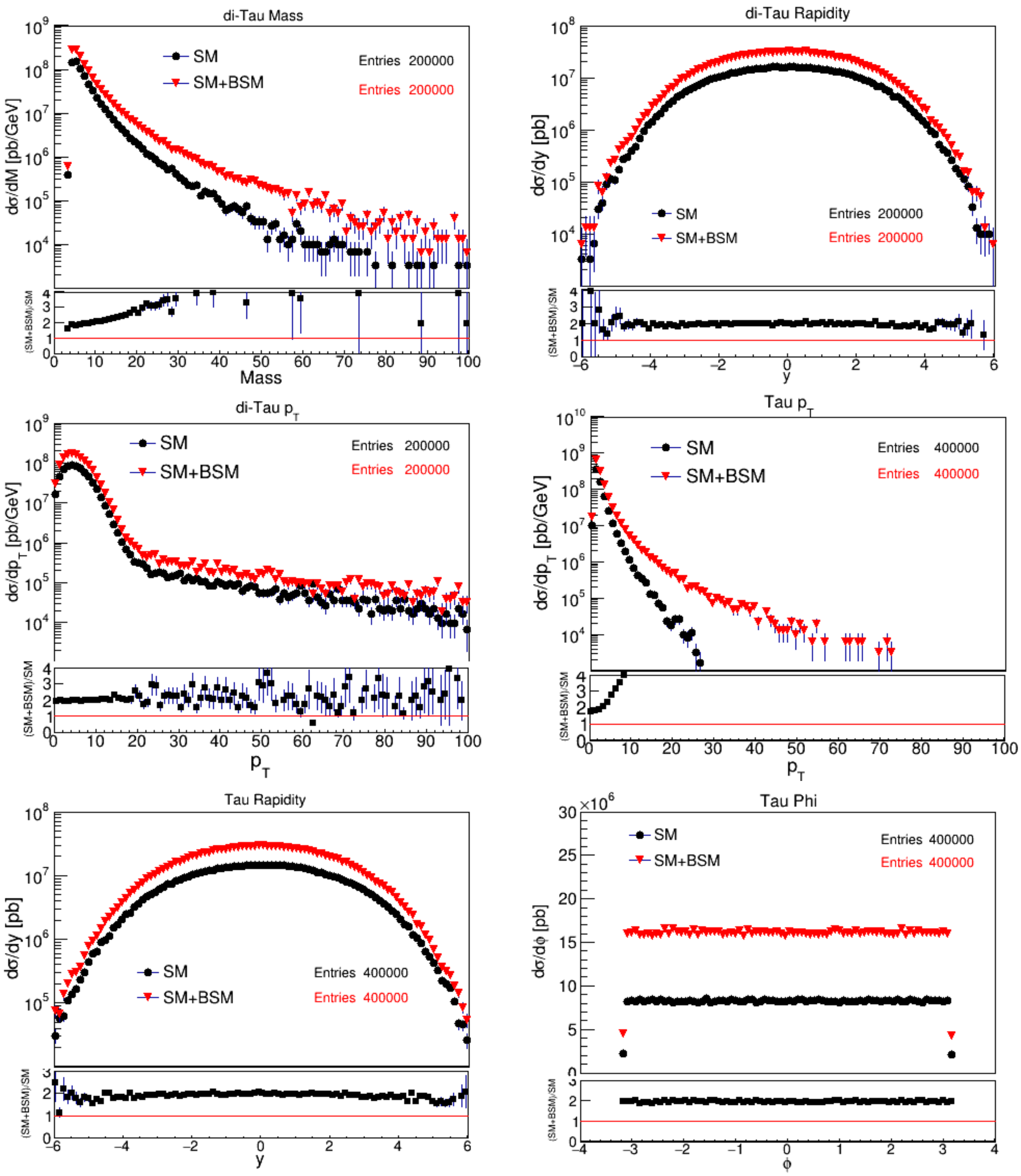

Figure 6: Two-tau system and single-tau distributions.

From the plots shown in Figure 7 it can be seen that the strong effects of $a_\tau = 0.2$ become less noticeable as we decrease, in magnitude, the value of a_τ. We plot the p_T and y distributions for $a_\tau = \pm 0.02$ and $a_\tau = \pm 0.05$. A negative value of a_τ produces a ratio of SM+BSM over SM lower than one which decreases as p_T increases. This means that if $a_\tau < 0$ we become less sensitive to higher p_T tau leptons than we are within the SM case ($a_\tau = 0$). On the other hand, even for $0 < a_\tau < 0.2$, we become more sensitive to higher p_T tau leptons when BSM physics is present.

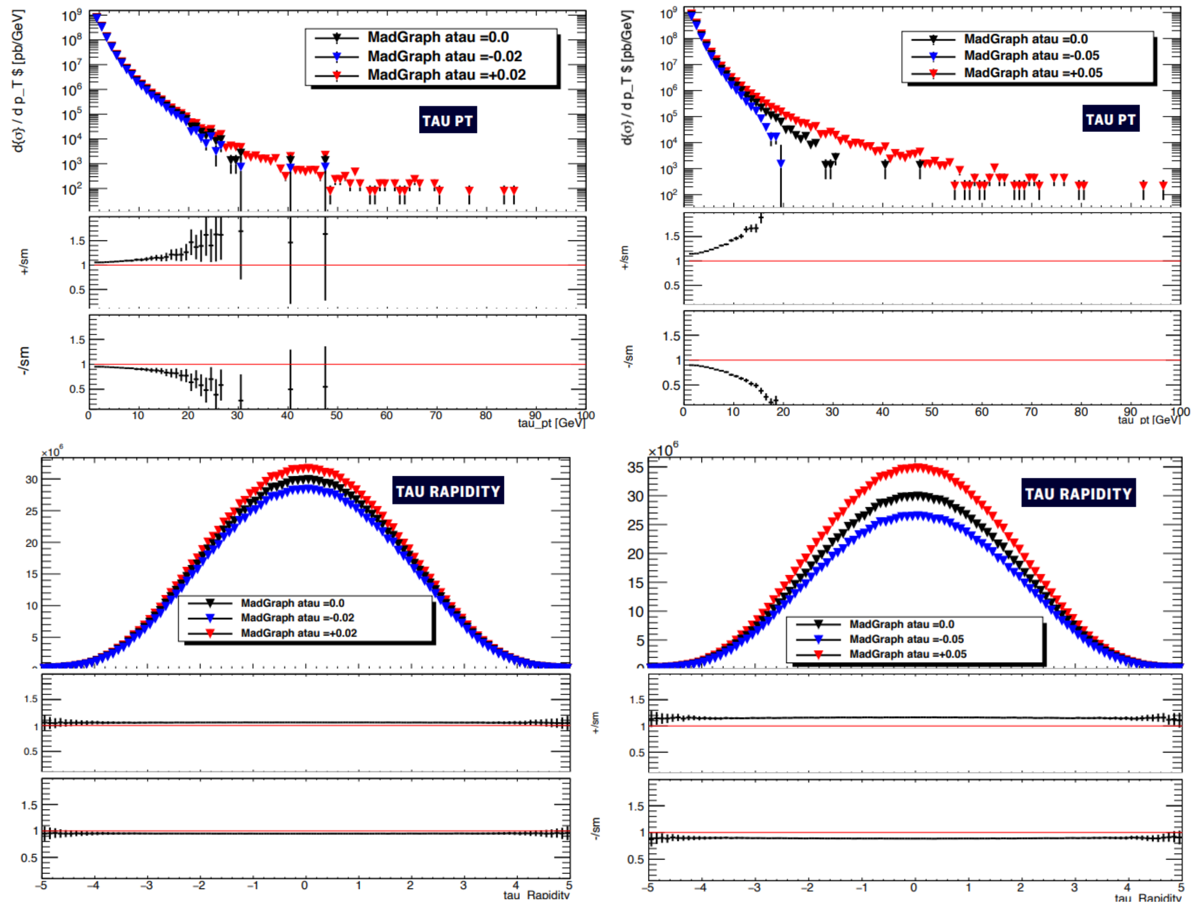

Figure 7: Transverse momentum and rapidity distributions for SM and SM+BSM samples with $a_\tau = \pm 0.02$ (left) and $a_\tau = \pm 0.05$ (right).

Finally, Figure 8 shows a significant correlation between the rapidities of the taus from the simulated tau pairs, which tend to be similar, i.e. they define a collimated beam.

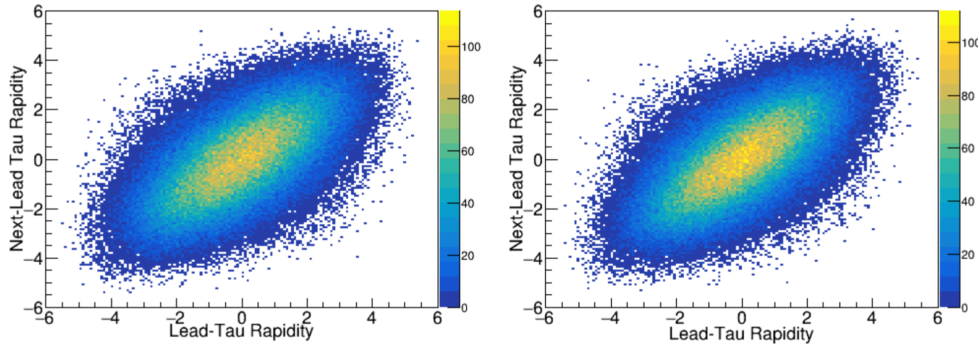

Figure 8: Correlation between the rapidities of the taus from the simulated tau pairs for the SM sample (left) and the SM+BSM sample (right).

4.3. Evaluation of τ decays in the fiducial volume

In the following section we look at some distributions for the generated f.s.p subject to fiducial constraints of the ATLAS detector (see Ref. [2]). We first require that at least one of the taus in $\gamma\gamma \rightarrow \tau^+\tau^-$ decay leptonically and then that the leading electron or muon satisfies the conditions $p_T > 4\ GeV$ and $|\eta| < 2.5$. Figure 9 shows correlations between properties of the taus and some of their decay products for the SM and SM+BSM samples.

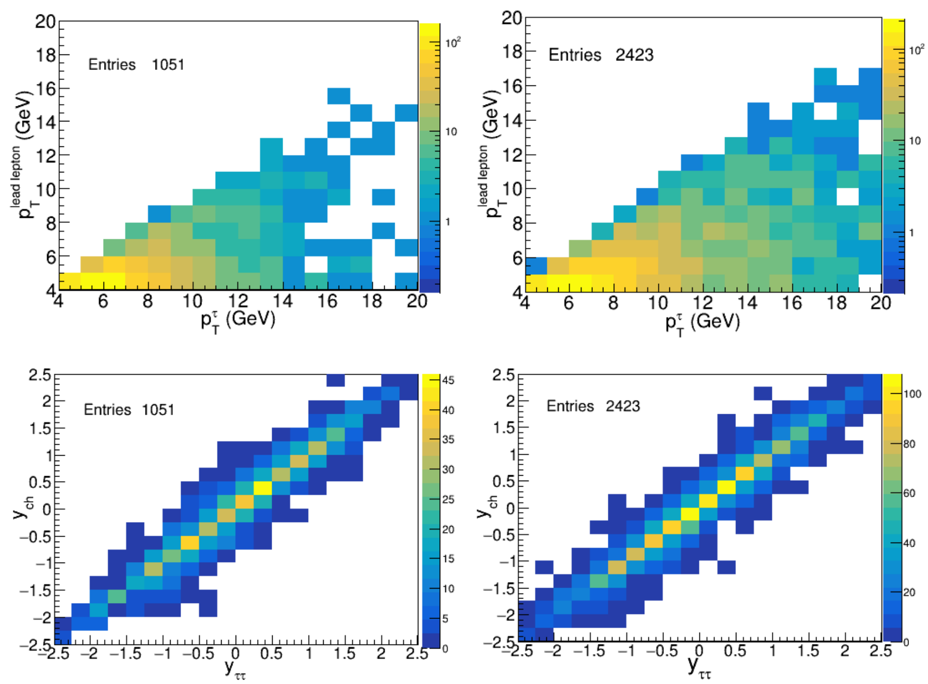

Figure 9: (Top row) Correlation between the p_T of the τ that decays leptonically and the p_T of the lepton it decays into. (Bottom row) Correlation between the rapidities of the tau system and the final-state charged particle system. The left column plots are obtained from the SM sample and the right ones from SM+BSM, and for all of them the fiducial cuts were applied.

The number of events that satisfy the fiducial constraints among the SM+BSM sample is more than two times the number for the SM sample, meaning that $a_\tau = 0.2$ (compared to $a_\tau = 0$ for SM) increases considerably the sensitivity we have to final state charged particles. This is mostly because the SM+BSM sample has much more taus and f.s.p at high p_T, as can be seen from the distributions shown in the top row of Figure 9. For both samples, there is a strong correlation between the rapidity of the tau system and the rapidity of the final state charged particle system. This could be used as a test to verify how likely it is for our reconstruction of the charged particles and the corresponding parent taus to have been carried out correctly.

The two main processes allowed considering the fiducial constraints specified above consists on one tau decaying leptonically and the other into a single charged particle ($\tau_l\tau_{1ch}$) or into three charged particles ($\tau_l\tau_{3ch}$). The first category is the one that can actually be confused with the $\gamma\gamma \to e^+e^-/\mu^+\mu^-$ background processes because of the signature they leave on the tracking system. In order to reject the background e^-/μ^- we keep only decays for which the vectorial sum of the transverse momenta of the decay products of the two tau leptons (lepton and either a second lepton or a pion) is greater than 1 GeV ($p_T^{l+1ch} > 1\ GeV$). In Figure 10 we show the distributions for electron and muons of the computed p_T^{l+1ch} upon which the background subtraction condition is based. There is a clear separation between signal and background distributions, explaining the good performance achieved by this filtering constraint.

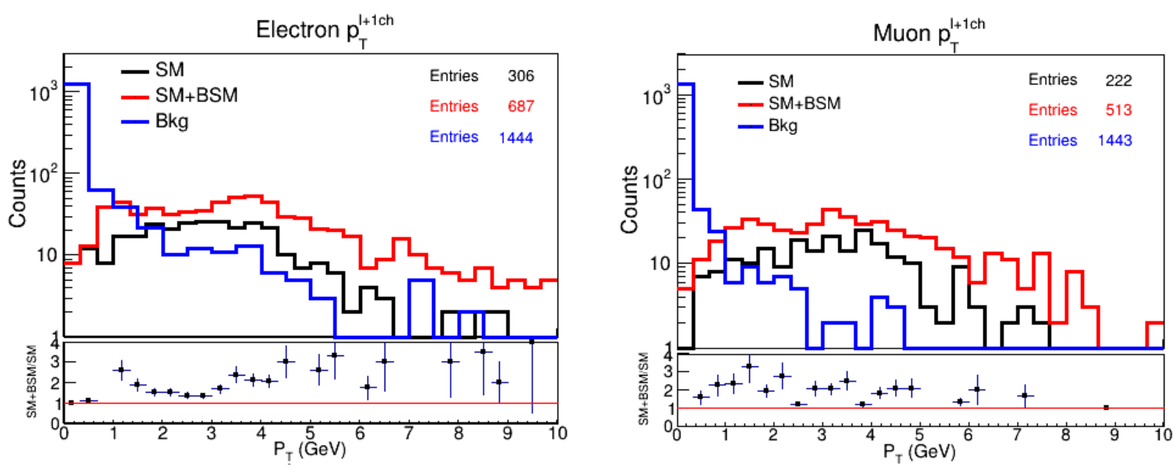

Figure 10: p_T^{l+1ch} distribution for electrons and muons.

The plots in Figure 11 compares the p_T distributions for final state electrons and muons among the SM, SM+BSM and Bkg samples when no cuts are applied, when fiducial cuts are applied and when fiducial cuts and the extra requirement $p_T^{l+1ch} > 1\ GeV$ are applied.

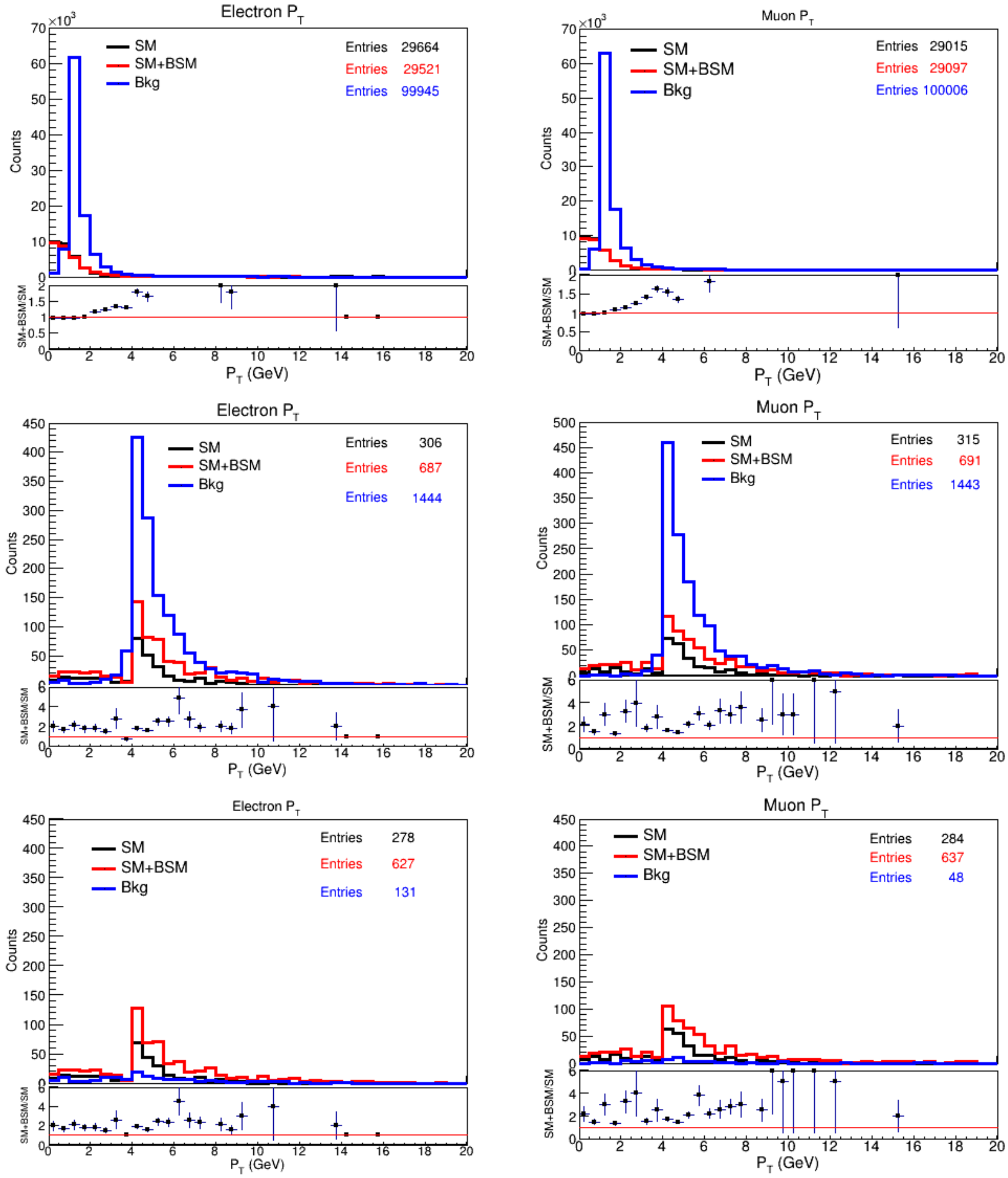

Figure 11: p_T distributions for electrons and muons among the SM, SM+BSM and Bkg samples with no constraints (top row), with fiducial cuts (middle row) and with further $p_T^{l+1ch} > 1\ GeV$ requirement (bottom row).

We don't have background processes for positive pions, but Figure 12 shows what happens to their p_T distribution when we apply the fiducial constraints and then add the condition $p_T^{l+1ch} > 1\ GeV$.

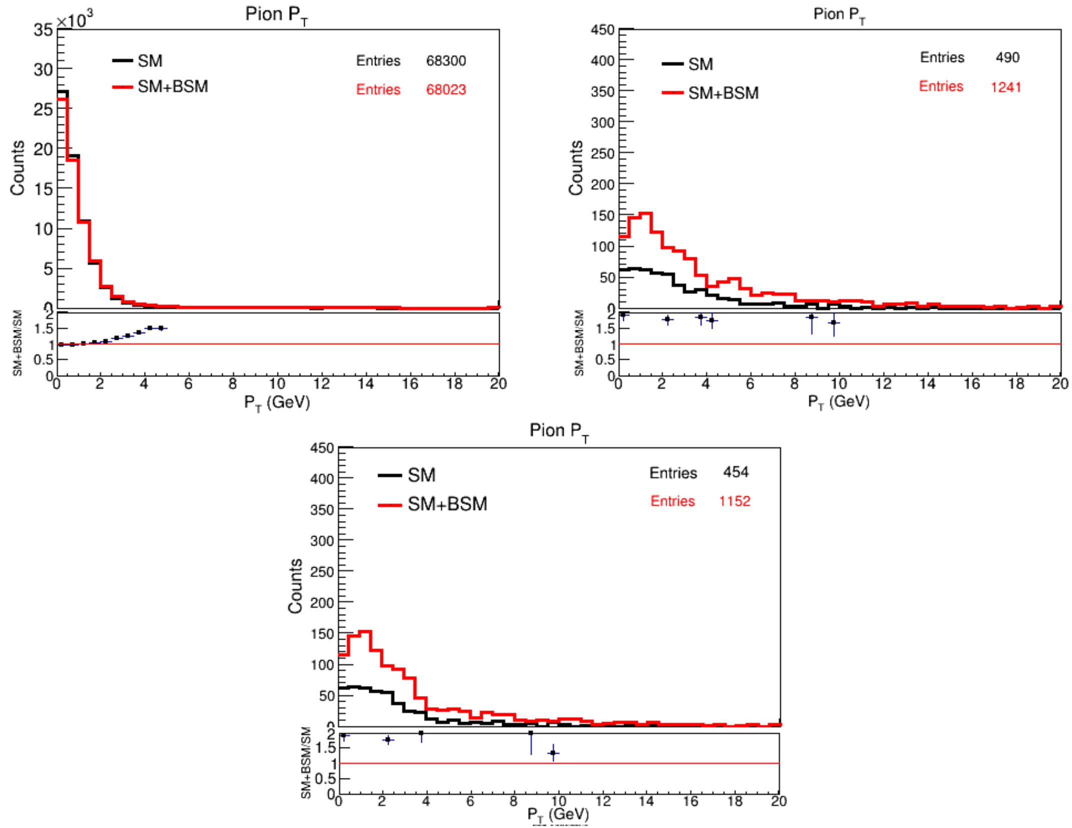

Figure 12: p_T distributions for pions among the SM, SM+BSM and Bkg samples with no constraints (top row), with fiducial cuts (middle row) and with further $p_T^{l+1ch} > 1\ GeV$ requirement (bottom row).

By applying the fiducial cuts on the unconstrained p_T distributions there is a huge reduction in the number of f.s.p mainly at $p_T < 4.0\ GeV$ affecting all samples similarly. However, by applying the extra requirement $p_T^{l+1ch} > 1\ GeV$ there is an almost absolute reduction in the background final state particles while the signal distributions are almost untouched. The specific fractions of f.s.p excluded by each constraint and each f.s.p type are specified in Table 9, and happen to be very similar for all studied particle types (e^-, μ^- and $\pi^{\pm}$).

Particle	e^-			μ^-			$\pi^{\pm}$	
Sample	SM	+BSM	Bkg	SM	+BSM	Bkg	SM	+BSM
(1) No cuts	29,664	29,521	99,945	29,015	29,097	100,006	68,300	68,023
(2) Fid. cuts	306	687	1,444	315	691	1,443	490	1,241
(3) Fid. cuts + $p_T^{l+1ch} > 1\ GeV$	278	627	131	284	637	48	454	1,152
(1) → (2) (%)	-99	-98	-99	-99	-98	-99	-99	-98
(2) → (3) (%)	-9	-9	-91	-10	-8	-97	-7	-7

Table 8: Number of f.s.p and their fractional reduction due to fiducial cuts applied to unconstrained distributions ((1)→(2)) and due to the further requirement $p_T^{l+1ch} > 1\ GeV$ ((2)→(3)). Here "+BSM" abbreviates "SM+BSM".

Figure 13 shows the fiducial cross sections as function of the leading lepton p_T for the SM and SM+BSM samples and for three different categories. All of them involve one of the two taus decaying leptonically (τ_l) but the other can decay into another lepton ($\tau_l\tau_{1ch=lepton}$), a charged pion ($\tau_l\tau_{1ch=\pi}$) or three charged pions ($\tau_l\tau_{3ch}$).

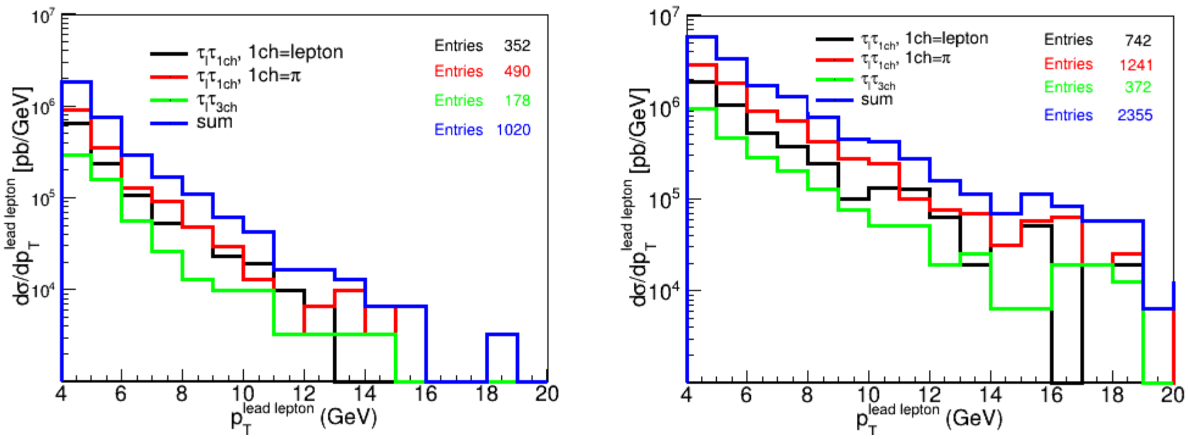

Figure 13: Fiducial cross section as a function of the p_T of the leading lepton for the SM (left) and SM+BSM (right) samples.

The most common process satisfying the fiducial constraints corresponds to one tau decaying leptonically and the other into a single charged pion. The second most common one is both tau leptons decaying leptonically. This is quantified in Table 10, which shows the integrated fiducial cross sections for each of these three categories.

Category	σ_{SM} (nb)	σ_{SM+BSM} (nb)
$\tau_l\tau_{1ch=l}$	1,141	4,681
$\tau_l\tau_{1ch=\pi}$	1,588	7,829
$\tau_l\tau_{3ch}$	577	2,347

Table 9: Integrated fiducial cross sections for the three most common decays of the tau lepton pair.

5. Summary and conclusion

We present a study of the kinematic characteriastics of the $\gamma\gamma -> \tau^+\tau^-$ process produced in the ultraperipheral collisions of the ion-leads produced in the LHC collider. These events can be used to obtain an indirect measurement of the tau anomalous magnetic moment or to improve the present limit of the a_τ parameter. We produced events generated with a combination of MadGrapH, Pythia8 and DELPHES for SM and SM+BSM processes as well as for the most abundant leptonic background.

Few validation checks have been carried out to verify that the simulated data-set and the analysis code were consistent. We measured the tau leptons branching fractions and the tracking efficiency for some f.s.p to verify consistency with the expected values from the PDG for the branching fractions and from the DELPHES data-card for the tracking efficiencies.

We have then started a comparison between the kinematic distributions for the SM, SM+BSM and bkg data-sets. Regarding the final state electrons and muons from the signal ($\gamma\gamma \to \tau^+\tau^- \to e^+e^-/\mu^+\mu^-$) and background ($\gamma\gamma \to e^+e^-/\mu^+\mu^-$) processes, we have found a clear difference in the shape of their p_T distributions. The electrons and muons coming from tau decays are predominantly softer than the ones produced in the back-to-back background process. Also, for all the f.s.p analyzed, the p_T distribution of the SM+BSM sample has systematically more particles at higher p_T than the SM sample, i.e. the ratio between SM+BSM over SM is increasingly greater than one for higher p_T.

The kinematics of tau leptons involved in the signal process has also been analyzed. It has been found that the ratio of the differential cross sections for the SM+BSM sample over the SM sample is mostly flat and centered at two for the di-tau p_T and y and the single-tau ϕ and y. On the hand, for the di-tau M and the single-tau p_T this ratio starts at two and increases for higher p_T. This means that we are at least two times more sensitive to tau decays when the BSM effects due to $a_\tau = 0.2$ are included. However, as the value of a_τ becomes smaller (e.g. $a_\tau = 0.02$ and $a_\tau = 0.05$) so does the differential cross section, and if a_τ becomes negative we get less sensitive to taus subject to BSM effects than we are when $a_\tau = 0$.

When imposing the fiducial constraints of the ATLAS detector we lose between 98-99% of the generated f.s.p in both signal and background samples. However, by requiring that these f.s.p satisfy the constraint $p_T^{l+1ch} > 1\ GeV$ we have been able to exclude 91-97% of the background, while reducing the signal in only 7-9%. A more complete study of how well we can separate our signal from background could be achieved by introducing other background processes such as $\gamma\gamma \to q\bar{q} \to f.s.p.$

To sum up, the distributions of the different observables studied here are clearly sensitive to the BSM physics introduced by the anomalous magnetic dipole moment of the tau lepton, and serve as promising mechanisms that can contribute to the indirect studies of a_τ.

References

[1] L. Beresford and J. Liu, "New physics and tau $g-2$ using LHC heavy ion collisions," Phys. Rev. D **102** (2020) no.11, 113008 doi:10.1103/PhysRevD.102.113008 [arXiv:1908.05180 [hep-ph]].

[2] M. Dyndal, M. Klusek-Gawenda, M. Schott and A. Szczurek, "Anomalous electromagnetic moments of τ lepton in $\gamma\gamma \to \tau^+\tau^-$ reaction in Pb+Pb collisions at the LHC," Phys. Lett. B **809** (2020), 135682 doi:10.1016/j.physletb.2020.135682 [arXiv:2002.05503 [hep-ph]].

[3] J. de Favereau *et al.*, "DELPHES 3, A modular framework for fast simulation of a generic collider experiment," JHEP **02** (2014), 057 doi:10.1007/JHEP02(2014)057 [arXiv:1307.6346 [hep-ex]].

[4] R. Corke and T. Sjostrand, "Multiparton Interactions and Rescattering," JHEP **01** (2010), 035 doi:10.1007/JHEP01(2010)035 [arXiv:0911.1909 [hep-ph]].

[5] J. Alwall, R. Frederix, S. Frixione, V. Hirschi, F. Maltoni, O. Mattelaer, H. S. Shao, T. Stelzer, P. Torrielli and M. Zaro,"The automated computation of tree-level and next-to-leading order differential cross sections, and their matching to parton shower simulations," JHEP **07** (2014), 079 doi:10.1007/JHEP07(2014)079 [arXiv:1405.0301 [hep-ph]].

[6] Rene Brun and Fons Rademakers, "ROOT - An Object Oriented Data Analysis Framework", Proceedings AIHENP'96 Workshop, Lausanne, Sep. 1996, Nucl. Inst. & Meth. in Phys. Res. A 389 (1997) 81-86. See also "ROOT" [software], Release v6.24/02, 29/06/2021, (Select the right link for your release here: `https://zenodo.org/search?page=1&size=20&q=conceptrecid:848818&all_versions&sort=-version`).

[7] P.A. Zyla *et al.* [Particle Data Group],"Review of Particle Physics," PTEP **2020** (2020) no.8, 083C01 doi:10.1093/ptep/ptaa104

[8] R. Escribano and E. Massó *et al.*, "New bounds on the magnetic and electric moments of the tau lepton", Physics Letters B, volume 301,pages 419-422,1993,urlhttps://www.sciencedirect.com/science/article/pii/037026939391172J,

[9] Fermilab. (2021, April 7). "First results from Fermilab's Muon g-2 experiment strengthen evidence of new physics", https://news.fnal.gov/2021/04/first-results-from-fermilabs-muon-g-2-experiment-strengthen-evidence-of-new-physics/

[10] T. Sjöstrand, S. Ask, J. R. Christiansen, R. Corke, N. Desai, P. Ilten, S. Mrenna, S. Prestel, C. O. Rasmussen and P. Z. Skands, "An introduction to PYTHIA 8.2," Comput. Phys. Commun. **191** (2015), 159-177 doi:10.1016/j.cpc.2015.01.024 [arXiv:1410.3012 [hep-ph]].

Appendix

A.1. MPI=ISR=on vs. MPI=ISR=off

Two important ingredients of the Pythia event generator are the *Initial State Radiation* and *Multiparton Interaction*. In this section we compare two SM samples, one with MPI and ISR turned "on" (MPI=ISR=on), and the other with both turned "off" (MPI=ISR=off). The plots contained in Figure 14 show th distributions of p_T and y distributions for generated final state e^-, μ^-, π^+. For the p_T plots we separate the f.s.p MPI=ISR=on according to whether they come or not from tau decays.

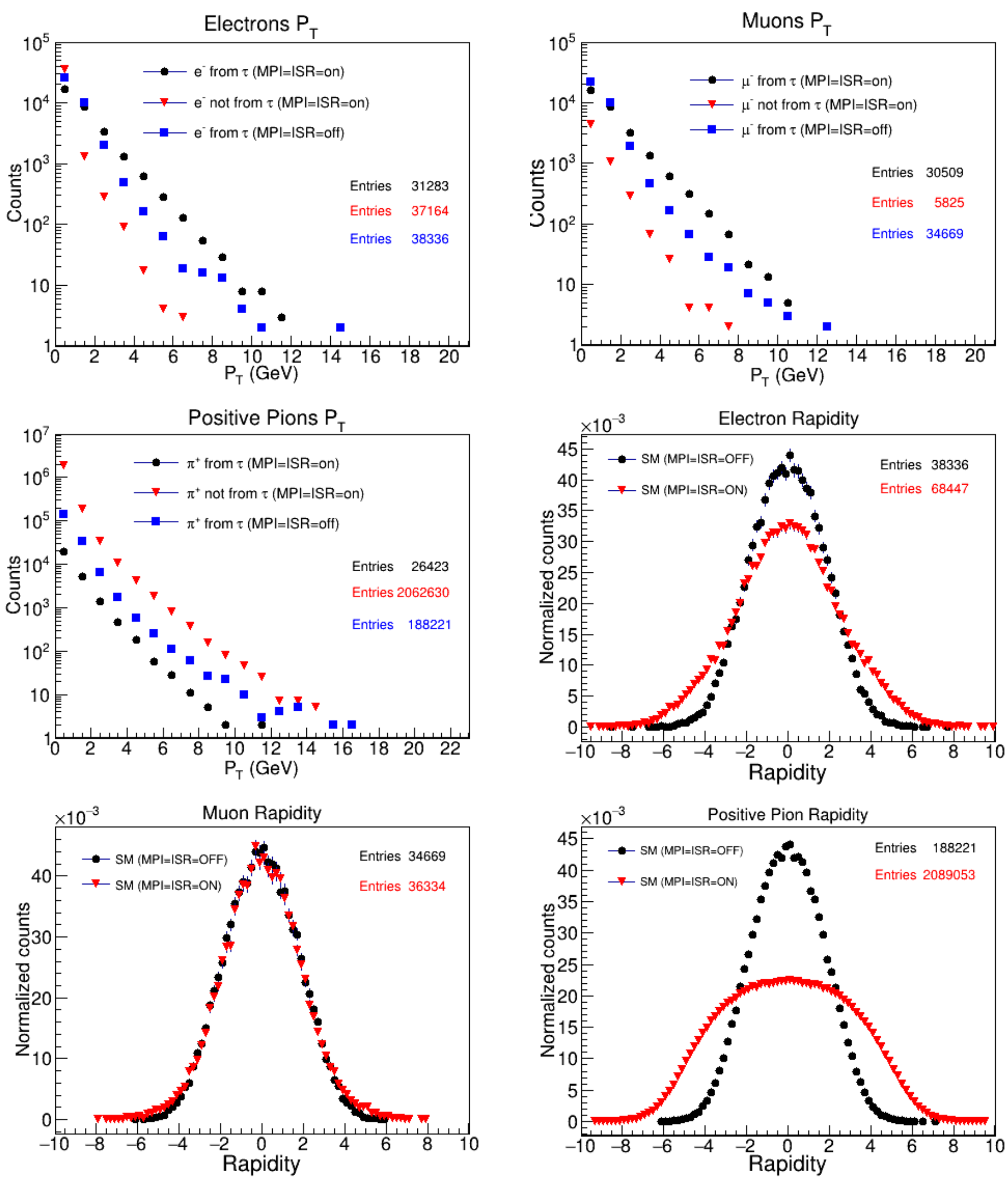

Figure 14: Electron, muon and positive pion transverse momentum and rapidity for the SM samples with MPI=ISR=on/off at generator level.

Figure 14 shows that final state electrons and muons not coming from tau decays are softer in p_T. For both samples the f.s.p are predominantly below the $P_T = 20\ GeV$ threshold. The rapidity distribution is wider for the MPI=ISR=on sample, while the MPI=ISR=off sample is practically constrained to $|y| < 5.0$.

In order to understand the effects that MPI+ISR=on has on the simulated sample we can start by comparing the type of processes that are included on each of the two samples. To do this we print the PID numbers (see Ref [7]) of the particles involved in the decay chain of the simulated events. Table 4 shows representative examples obtained from the MPI=ISR=on sample.

Particle	PID
e^-	11
μ^-	13
τ^-	15
π^+	211
γ	22
g	21
d	1
u	2
p	2212

f.s.p	e^-			μ^-		π^+		
	2212	2212	2212	2212	2212	2212	2212	2212
	2	1	21	21	1	2	22	2
	22	22	3	-1	-413	22	22	223
PID	15	22	111	22	-411	22	15	211
	11	-15	11	22	13	-15	-311	
		311		15		211	310	
		310		13			211	
		111						
		11						

Table 10: PDG numbers for some particles (left) and some example decay chains (time going down the rows) for different final state particles as simulated by Pythia8 for MPI=ISR=on (right).

As it can be seen from Table 4, in the MPI=ISR=on sample we can have f.s.p coming from tau decays directly or indirectly (first and second subcolumns for each f.s.p) or from a chain of decays that don't involve any tau or photon. For the MPI=ISR=off we have processes of the first and second type, but no chain of decays that don't start with tau production from photon fusion followed by decays into f.s.p. This means that the MPI=ISR=on sample includes an independent source of f.s.p due to MPI and ISR (not involving the simulated process of gamma fusion into a pair of taus). Therefore, in order to have a clean signal-only sample to study the $\gamma\gamma \to \tau^+\tau^- \to f.s.p$ we choose MPI=ISR=off.

A.2. Pythia8 run card

```
## Config for Py8 with NNPDF23 QED pdf

include("Pythia8_i/Pythia8_Base_Fragment.py")

genSeq.Pythia8.Commands += [
  "PDF:pSet= LHAPDF6:NNPDF23_nnlo_as_0118_qed",
    "SpaceShower:rapidityOrder = on",
    "SigmaProcess:alphaSvalue = 0.140",
    "SpaceShower:pT0Ref = 1.56",
    "SpaceShower:pTmaxFudge = 0.91",
    "BeamRemnants:unresolvedHadron=3",
    "SpaceShower:pTdampFudge = 1.05",
    "SpaceShower:alphaSvalue = 0.127",
    "TimeShower:alphaSvalue = 0.127",
    "SpaceShower:pTdampMatch = 1",
    "BeamRemnants:primordialKThard = 0.1",
    "BeamRemnants:primordialKTsoft=0.1",
    "PartonLevel:MPI = off",
    "PartonLevel:ISR = off",
    "SpaceShower:pTmaxMatch = 1",
    "SpaceShower:pTmaxFudge = 1.",
    "TimeShower:pTmaxMatch = 1",
    "TimeShower:pTmaxFudge = 1.",
    "SpaceShower:MEcorrections = off",
     "TimeShower:MEcorrections = off",
     "TimeShower:globalRecoil = on",
     "TimeShower:weightGluonToQuark = 1" ,
     "BeamRemnants:primordialKTremnant = 0.1"
]

evgenConfig.tune = "NNPDF23_QED"

#EvtGen for b fragmentation as default.  No EvtGen is available in "nonStandard"
include("Pythia8_i/Pythia8_EvtGen.py")
```

Figure 15: Pythia8 run card used to simulate decays, radiation and showering (among other things).